Electronic Supplementary Material (ESI) for RSC Advances.

Superior Elastomeric Nanocomposites with Electrospun Nanofibers and Nanoparticles of $CoFe_2O_4$ for Magnetorheological Applications

Bablu Mordina,[1, 2] Rajesh Kumar Tiwari,[1] Dipak Kumar Setua,[1,#] and Ashutosh Sharma[2,*]

[1]Defence Materials and Stores Research and Development Establishment, Kanpur-208013, India

[2]Department of Chemical Engineering & Center of Nanoscience, Indian Institute of Technology Kanpur, India

Supporting Information

Electrospinning:

Figure S1 shows the schematic of electrospinning setup used for nanofiber preparation.

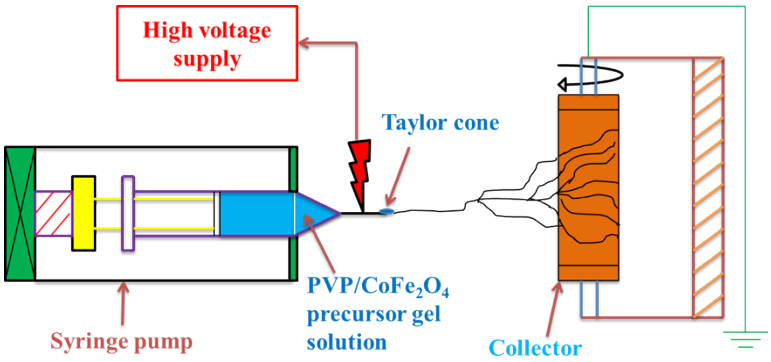

Figure S1: Schematic of electrospinning setup.

Curing reaction of Sylgard 184:

Sylgard 184 is available in two pack system. Part 1 contains base polymer, vinyl terminated oligomer (*i.e.* dimethylvinyl-terminated dimethyl siloxane) mixed with Pt based catalyst (generally H_2PtCl_6). Part 2 is a hydrogen containing silicone curing agent, dimethyl methylhydrogensiloxane. When part 1 and part 2 were mixed in the 10:1 weight ratio, chemical cross linking took place by the reaction of active –H with the terminal vinyl group of the oligomer leading to the highly three dimensional network structure by forming Si-CH_2-CH_2-Si bond.

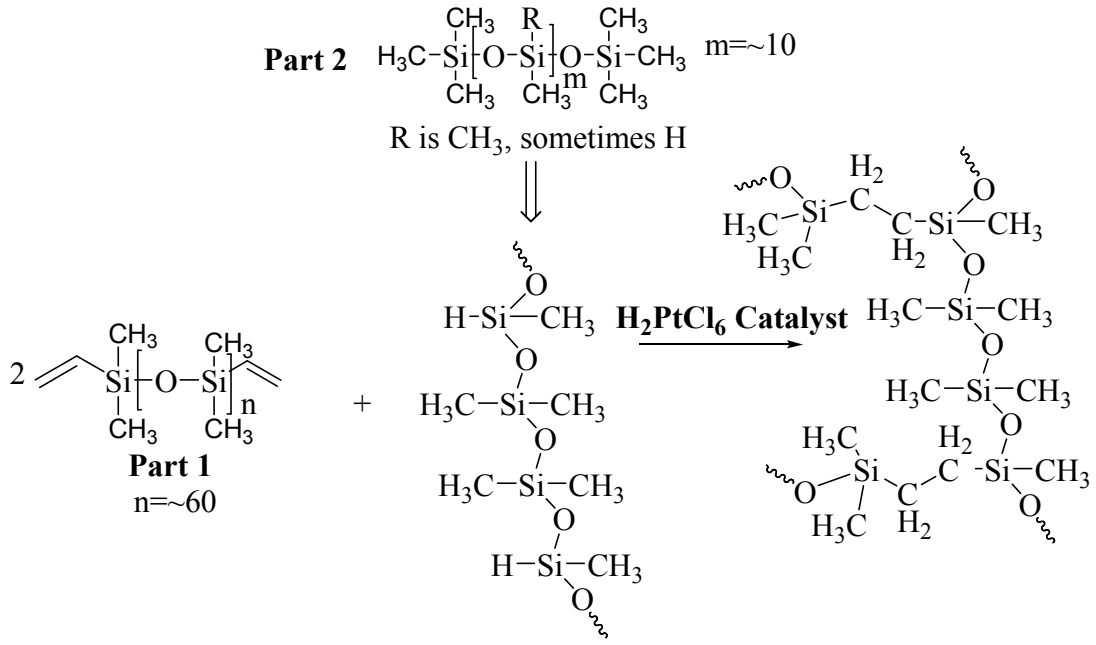

Scheme I: Curing reaction of Sylgard 184.

Fourier Transform Infrared (FT-IR) Spectroscopy:

FT-IR of Sylgard part 1 and part 2, neat PDMS and nanocomposites were performed in the wave number range 400 to 4000 cm^{-1} with a resolution of 4 cm^{-1} and an average of 24 scans was taken for recording of the spectra by using Perkin-Elmer FT-IR instrument (Model Spectrum 100). Figure S2 depicts that both Sylgard part 1 and part 2 show absorption peaks at 2962 and 2904 cm^{-1} due to asymmetric and symmetric stretching vibration of $–CH_3$ respectively. Absorption band at 1261 cm^{-1}can be attributed to the symmetric deformation of $–CH_3$. Absorption peaks at 802 and 1096 cm^{-1} can be attributed to the Si-C asymmetric stretching in Si-CH_3 and Si-O-Si stretching vibration. Apart from these Sylgard part 1 and part 2 shows distinct signature peaks at 1598 and 2162 cm^{-1} due to C=C stretching vibration of vinyl ($–CH=CH_2$) group and Si-H stretching vibration, respectively.

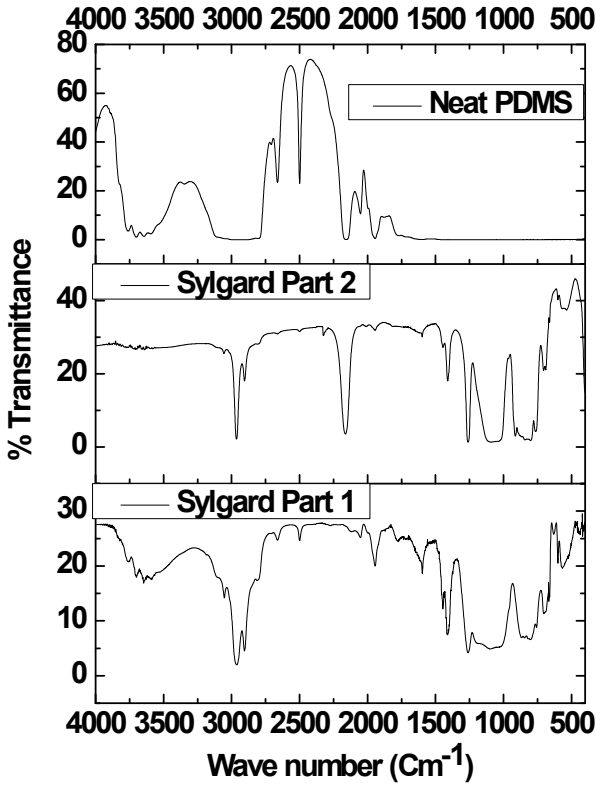

Figure S2: FT-IR of Sylgard 184 part 1, part 2 and cured neat PDMS film.

Curing is confirmed by the disappearance of absorption peaks corresponding to C=C (for Sylgard part 1) and Si-H (for Sylgard part 2) stretching vibration. Figure S2 and S3 exhibit that cured neat PDMS as well as all nanocomposite films show decrease in peak intensity of Si-H stretching vibration at 2162 cm^{-1} compared to that of pure Sylgard part 2 which confirms the curing reaction of Si-H with $–CH=CH_2$ to form $Si-CH_2-CH_2-Si$. Increase in the intensity of peak at 2499 cm^{-1} (overtone of symmetric deformation (IR absorption band at 1261 cm^{-1}) of $-CH_3$ group bonded with silicon) also firmly support the curing of PDMS elastomer. Moreover, broadening of peak at 2900-2962 Cm^{-1} indicates the presence of huge number of $–CH_3$ groups in cured polymer backbone (PDMS).

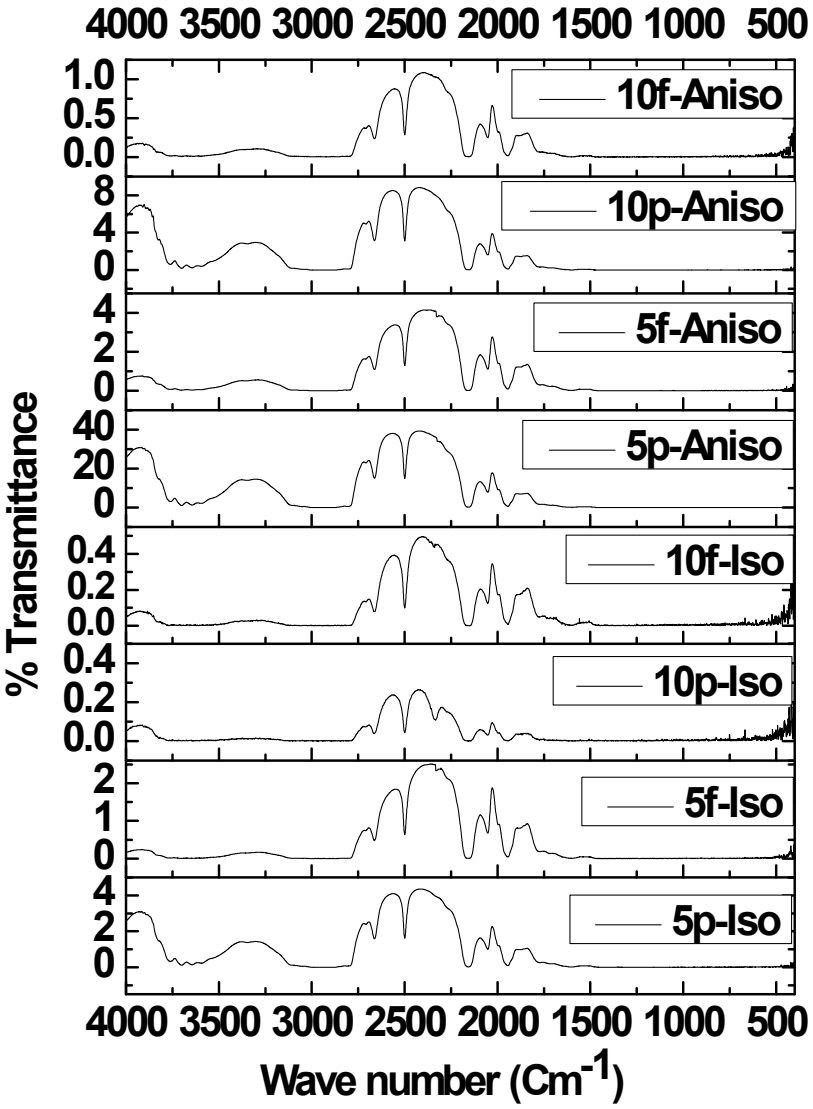

Figure S3: FT-IR of $CoFe_2O_4$ -PDMS nanocomposites (Note: numeral (5 or 10), p, f, Iso and Aniso indicate $CoFe_2O_4$ loading (wt%), nanoparticle, nanofiber, Isotropic and Anisotropic films, respectively).

VSM curves of nanocomposites:

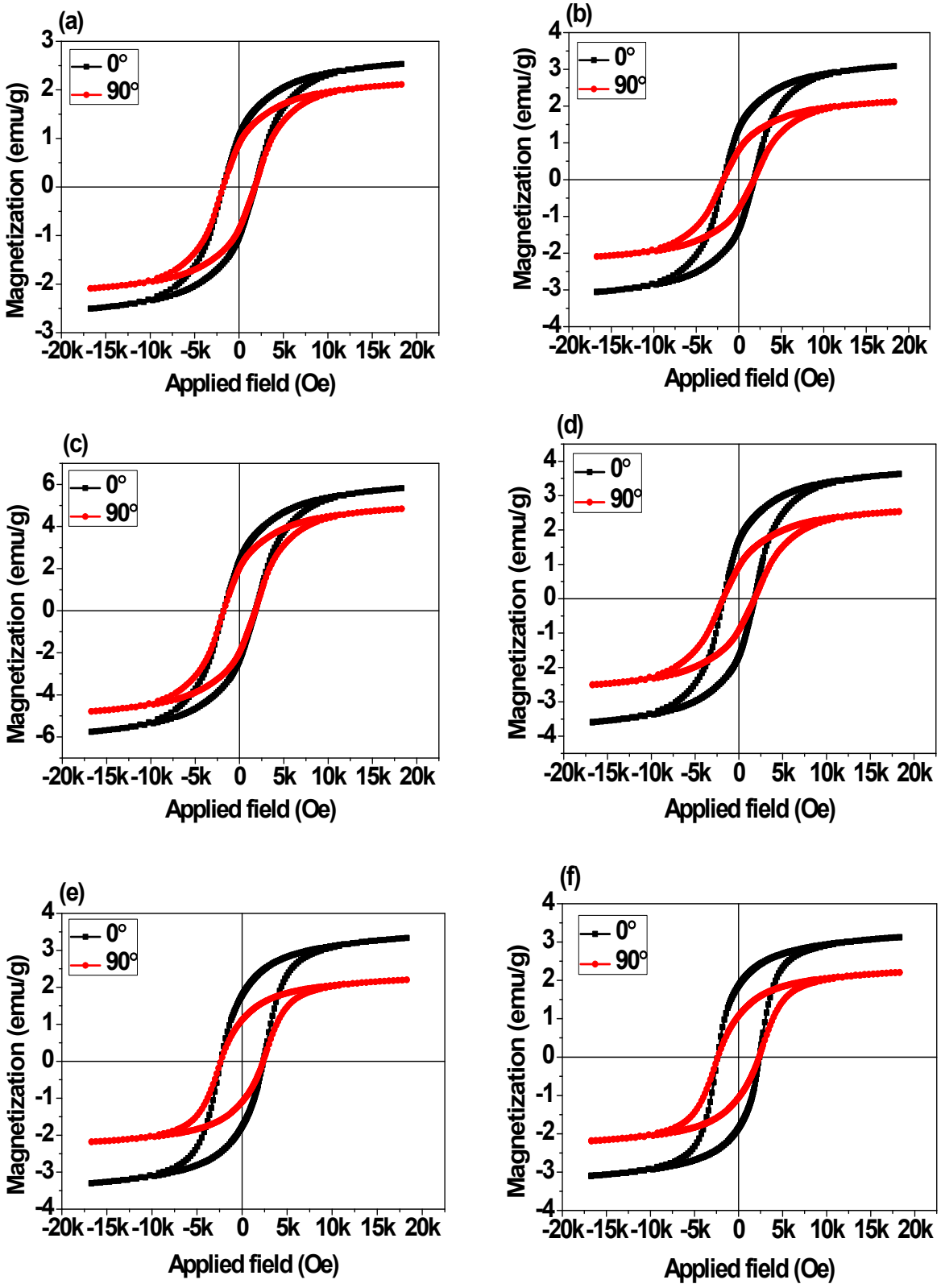

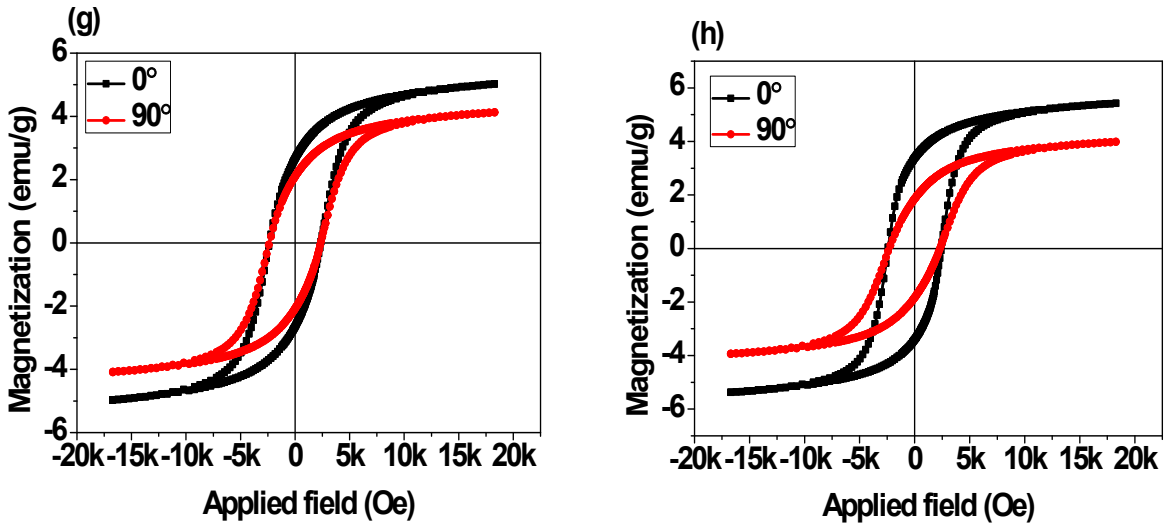

Figure S4: Hysteresis curves of p-$CoFe_2O_4$-PDMS nanocomposites (a) 5 wt. % Isotropic, (b) 5 wt. % Anisotropic, (c) 10 wt. % Isotropic, (d) 10 wt. % Anisotropic; f-$CoFe_2O_4$-PDMS nanocomposites (e) 5 wt. % Isotropic, (f) 5 wt. % Anisotropic, (g) 10 wt. % Isotropic, (h) 10 wt. % f Anisotropic.

FESEM:

Figures S5 (a), (c) and (e), (g) are the FESEM images of 5 and 10 wt. % isotropic p-$CoFe_2O_4$-PDMS NCs and f-$CoFe_2O_4$-PDMS NCs, respectively while Figures S5 (b), (d) and (f), (h) are that of respective anisotropic nanocomposites. It can be seen from the above images that the nanoparticles are embedded within the polymer matrix in the form of agglomerated particles. The formation of the fiber fragments joining to make chains is also evident on the surface of anisotropic nanocomposites. The figures indicate a good dispersion with randomly distributed fiber fragments in case of isotropic nanocomposites and oriented nanofiber chains along the direction of the magnetic field in anisotropic nanocomposites.

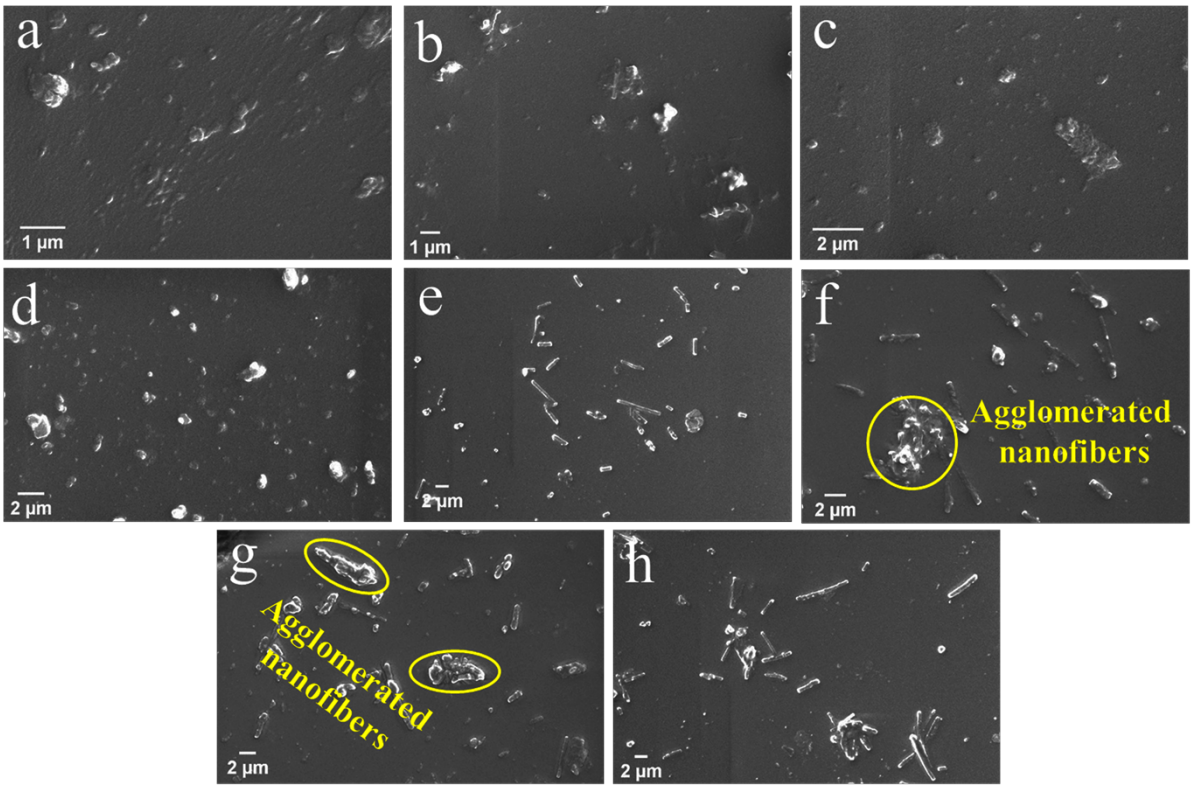

Figure S5: FESEM images of p-$CoFe_2O_4$-PDMS nanocomposites (a) 5w% Isotropic, (b) 5w% Anisotropic, (c) 10 wt. % Isotropic, (d) 10 wt. % Anisotropic; f-$CoFe_2O_4$-PDMS nanocomposites (e) 5 wt. % Isotropic, (f) 5 wt. % Anisotropic, (g) 10 wt. % Isotropic, (h) 10 wt. % Anisotropic.

Magnetorheology:

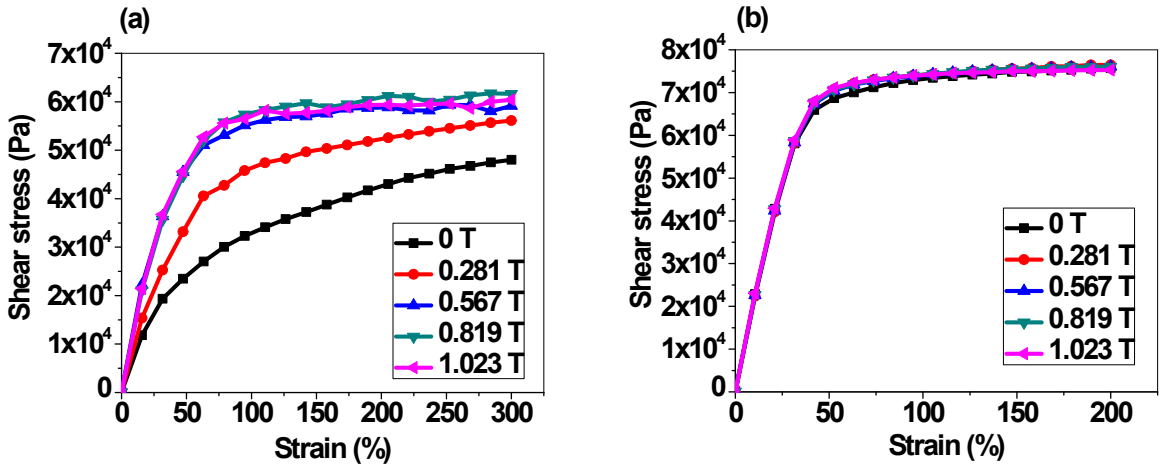

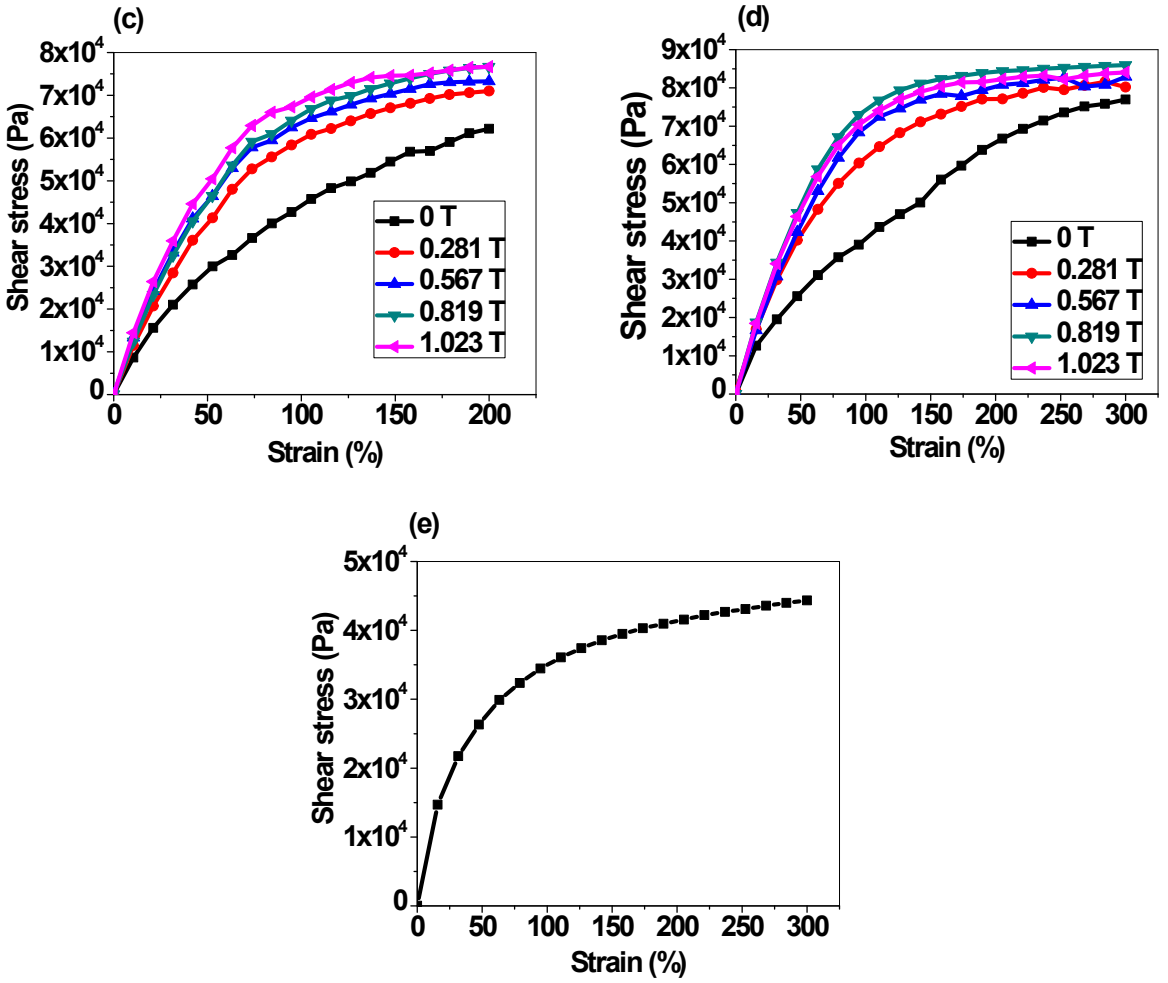

Figure S6: Shear stress vs. Shear strain curves of p-$CoFe_2O_4$-PDMS nanocomposites (a) 5 wt. % Isotropic, (b) 5 wt. % Anisotropic; f-$CoFe_2O_4$-PDMS nanocomposites (c) 5 wt. % Isotropic, (d) 5 wt. % Anisotropic; (e) Neat PDMS at 0 T.

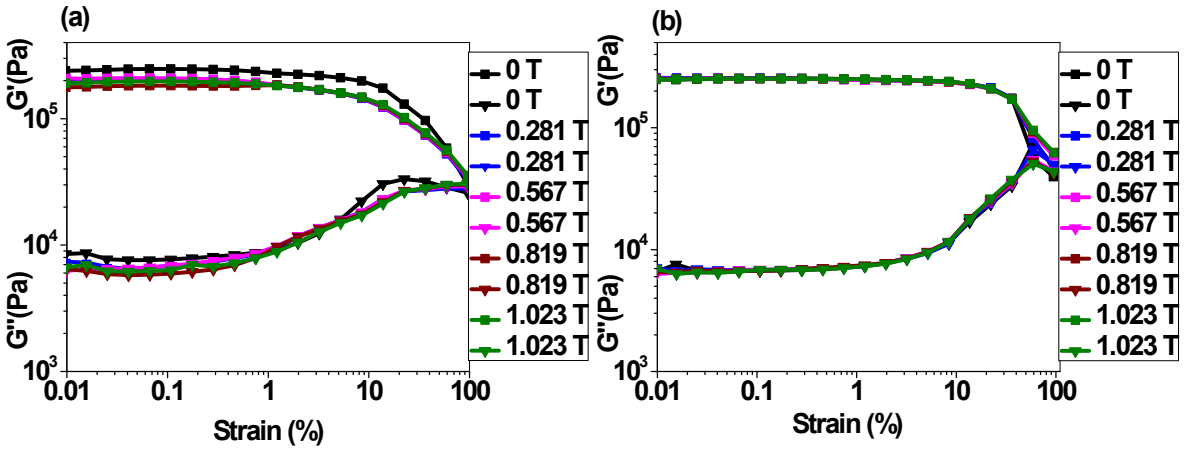

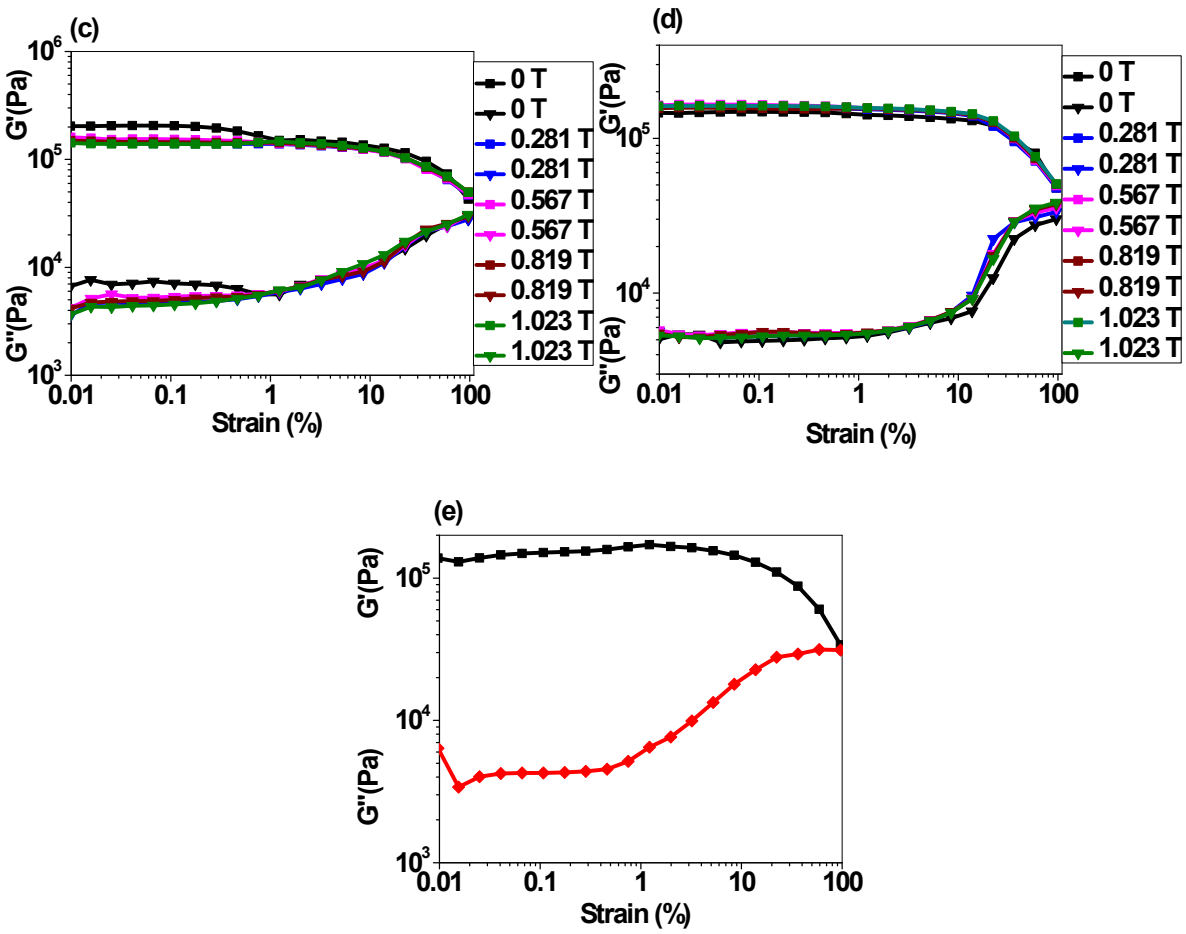

Figure S7: Strain sweep curves of p-$CoFe_2O_4$-PDMS nanocomposites (a) 5 wt. % Isotropic, (b) 5 wt. % Anisotropic; f-$CoFe_2O_4$-PDMS nanocomposites (c) 5 wt. % Isotropic, (d) 5 wt. % Anisotropic; (e) Neat PDMS at 0 T.

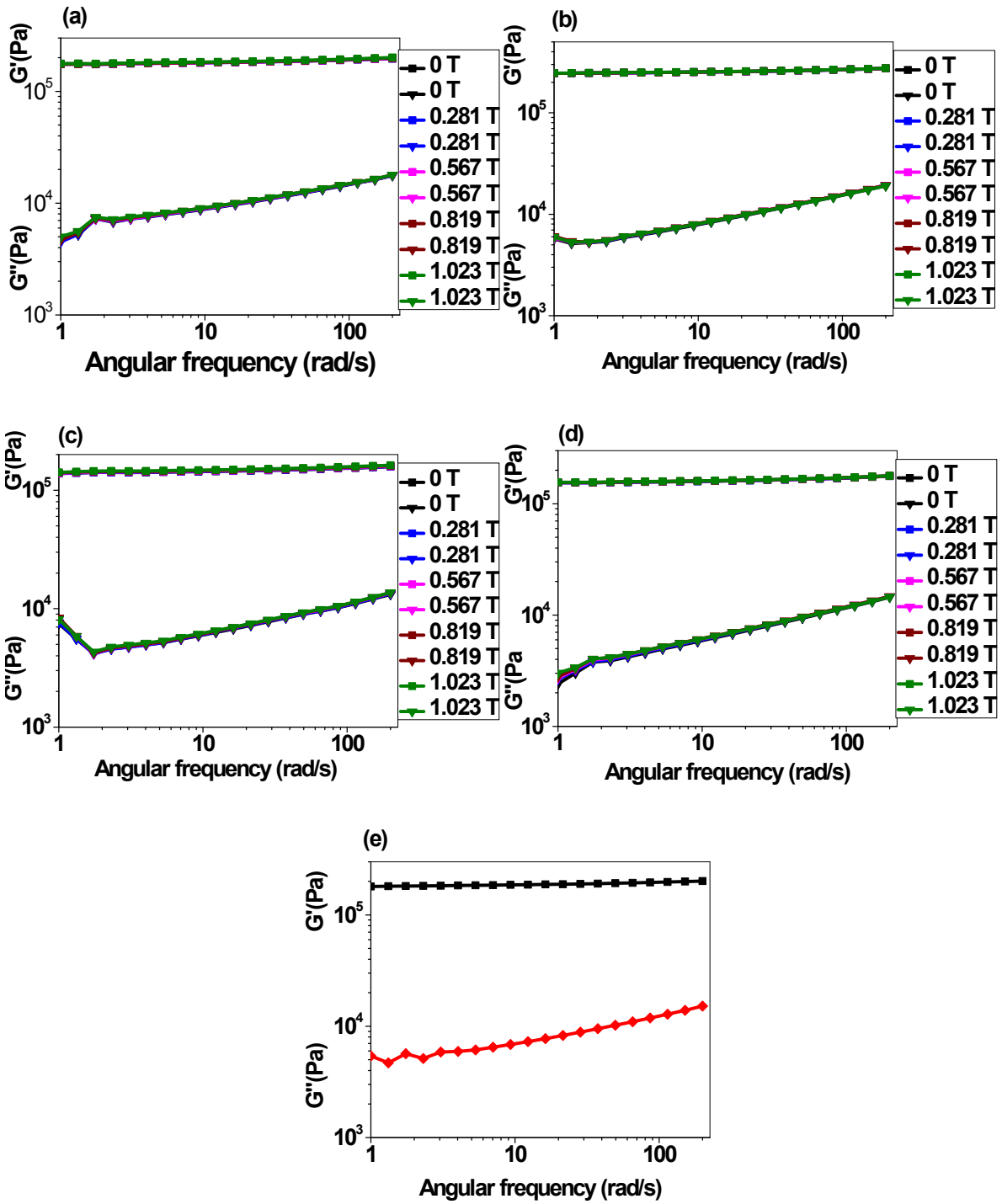

Figure S8: Angular frequency sweep curves of p-$CoFe_2O_4$-PDMS nanocomposites (a) 5 wt. % Isotropic, (b) 5 wt. % Anisotropic; f-$CoFe_2O_4$-PDMS nanocomposites (c) 5 wt. % Isotropic, (d) 5 wt. % Anisotropic; (e) Neat PDMS at 0 T.

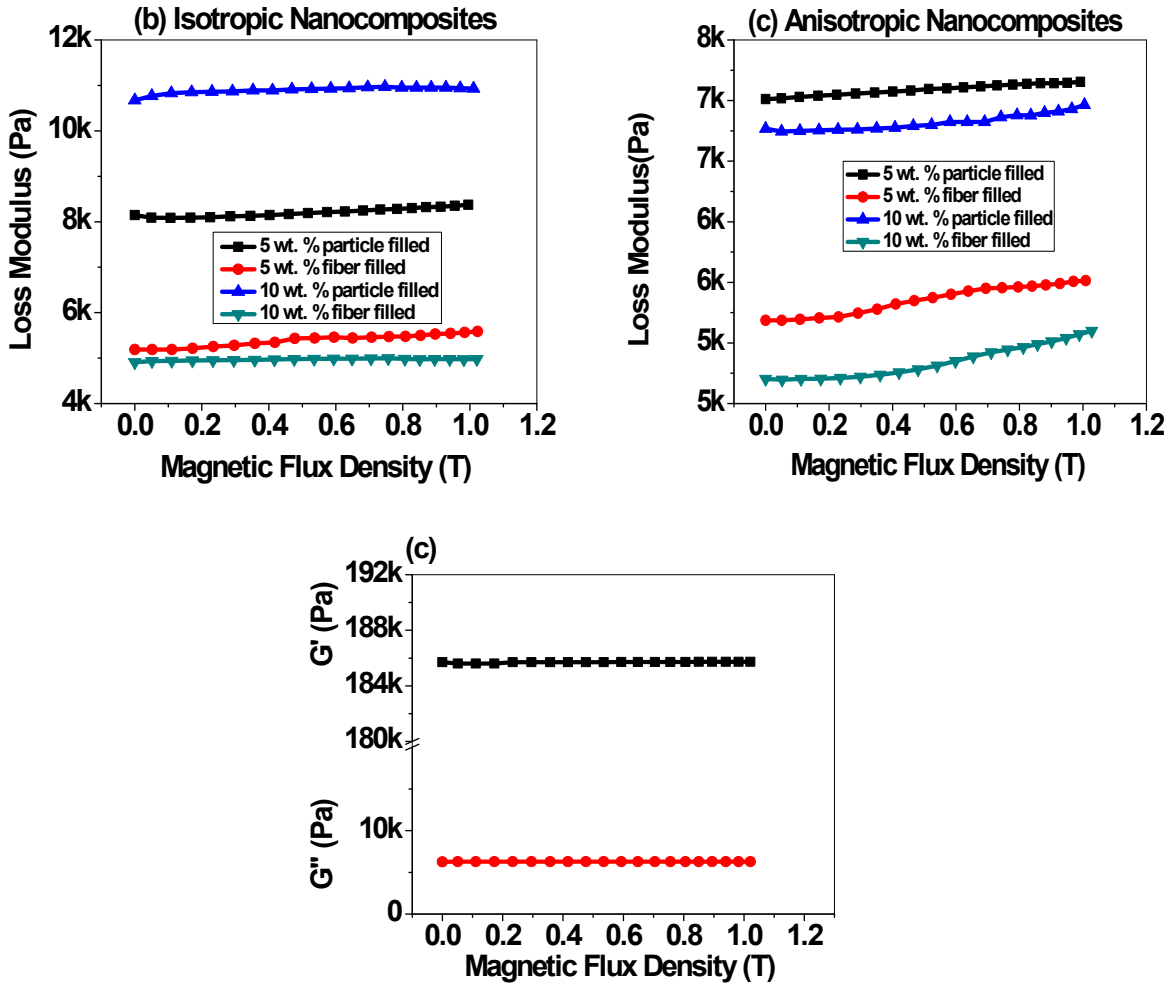

Figure S9: Loss modulus versus magnetic flux density curve of (a) isotropic nanocomposites, (b) anisotropic nanocomposites; (c) Storage and loss moduli versus magnetic flux density curves of Neat PDMS.